Available online at www.sciencedirect.com

ScienceDirect

IFAC PapersOnline CONFERENCE PAPER ARCHIVE

IFAC PapersOnLine 54-16 (2021) 63–69

Adaptive Backstepping Control of Ship Speed Tracking and Hybrid Mode Selection ⋆

Fan Gao * **Astrid H. Brodtkorb** * **Sigrid Marie Mo** **
Zhengru Ren *** **Asgeir J. Sørensen** *

* *Centre for Autonomous Marine Operations and System (AMOS), Department of Marine Technology, Norwegian University of Science and Technology, Trondheim, Norway (e-mail: fan.gao@ntnu.no, astrid.h.brodtkorb@ntnu.no, asgeir.sørensen@ntnu.no)*
** *Brunvoll AS, Molde, Norway (e-mail: Sigrid.Marie.Mo@brunvoll.no)*
*** *Department of Marine Technology, Norwegian University of Science and Technology, Trondheim, Norway (e-mail: zhengru.ren@ntnu.no)*

Abstract: This paper investigates the application of adaptive backstepping control to a hybrid power system for ship propulsion, using a main diesel engine in conjunction with a battery for auxiliary power supply. Fuel injection delay to the diesel engine is estimated based on Pade approximation, and the pure-feedback term in the ship speed dynamics is approximated by Radial Basis Function (RBF) Neural Network. The closed-loop system is proved to be uniformly ultimately bounded.

Keywords: Speed tracking, neural network approximation, backstepping design, hybrid power system, fuel injection delay.

1. INTRODUCTION

The mechanisation of ship propulsion was first formulated in the mid 19th century (Xiros, 2012). In the past many years, ship propulsion directly driven by engine sets has been widely applied for global shipping. Most ships use diesel engines as the main power source due to their high fuel efficiency at design engine speed (around 80% of top speed) and low particulate matter (PM) emissions. For ship operations in different power loading conditions, electrification has been a dominant trend for ship power and propulsion system to reduce propulsion-load fluctuations, improve efficiency, and reduce emissions. Therefore, hybrid ship power and propulsion system is coming into researcher's sight, stated in Geertsma et al. (2017). Recently, the usage of energy storage has become a popular trend for hybrid power supply system in Mestemaker et al. (2020). However, the application of purely stored power supply is restricted into short-range ships due to the limited storage capacity of batteries. The battery energy storage is, in another idea, used to store braking energy to run the engine in a more efficient operating point in Miyazaki et al. (2016). In this paper, a battery-auxiliary hybrid power system is introduced for high speed transit operations of ships.

In the ship propulsion system, the engine load control is achieved by varying the injected fuel per cycle. Vrijdag and Stapersma (2017) states that the fuel injection command is translated into the actual fuel injection within two revolutions in a 4-stroke diesel engine. Thus, during the controller design of ship propulsion system, a time delay must be considered to simulate this translation procedure. Pade approximation in Li et al. (2016) and auxiliary system in Ma et al. (2018) are introduced to compensate for the effect of input delay.

For pure-feedback nonlinear systems, approximation-based control has been widely used to tackle nonlinear characteristics existing in practical systems, stated by Ge and Wang (2002). The fuzzy concept and neural network approximation are introduced in the backstepping control strategy to handle unknown nonlinear systems. By combining fuzzy or neural network model with adaptive updating law, many satisfactory results have been presented in Li et al. (2016) and Ge and Wang (2002). The comparison of using RBF networks and fuzzy inference systems is discussed in Yu et al. (2011). Compared to the RBF networks, the fuzzy inference system is easier to be designed, but has lower accuracy of approximation. Besides, Liu and Tong (2016) proposed a barrier Lyapunov function-based adaptive backstepping control where the mean value theorem is used to to transform the pure-feedback systems to a strict-feedback structure with full state constraints.

This paper focuses on the interaction of ship speed dynamics and propulsion dynamics. The main contribution is the development of an adaptive backstepping control strategy to track the desired ship speed via controlling the fuel injection to the diesel engine, and the auxiliary electric power

⋆ This work was supported by the Research Council of Norway through the SEAOPS project of Brunvoll AS, project number 309660, and through the Centre of Excellence funding scheme, project number 223254, AMOS.

10.1016/j.ifacol.2021.10.074

supply for high speed. Only surge motion is considered and the interaction between the main propeller, rudder and other auxiliary thrusters are neglected. The paper is organised as follows. Section 2 provides the problem formulation, necessary notations and preliminaries. Section 3 introduces the adaptive backstepping controller design and stability analysis. Section 4 contains the simulation of the proposed ship propulsion system, and in Section 5, we conclude the work of the paper.

2. DYNAMIC MODEL OF THE HYBRID SHIP PROPULSION SYSTEM

The control objective of the ship propulsion system is to track a given ship speed. The mathematical formulation of the speed tracking system is stated in Section 2.1. In Section 2.2, several linearisation methods and simplification of the ship dynamics are introduced. Sections 2.3 and 2.4 describe the control of electric torque and the simulator settings.

2.1 System Modelling

Referring to the literature in Zhao et al. (2018), the model of the hybrid ship propulsion system considering surge degree of freedom only is given by (1). The proposed system contains three main dynamic system: ship speed (v), engine speed ($\omega_e = 2\pi n_e$) and engine torque (M_e). The control input is the fuel injection X. Due to the injection delay, a time delay τ_d is introduced into the input.

$$M\dot{v} = F_p - F_r + F_e \tag{1a}$$
$$I\dot{\omega}_e = M_e + M_b - M_p - M_f \tag{1b}$$
$$T\dot{M}_e = -M_e + KX(t-\tau_d) \tag{1c}$$

where M is the ship mass including added mass, I is the moment of inertia of the shaft system, F_p and F_r denote the ship propeller thrust and ship resistance respectively, F_e is the environmental force which is neglected. The torque M_e is the torque delivered by the engine, M_p is the torque from the propeller, M_f denotes the frictional torque, and M_b is the torque supplied by the battery and electric motor system.

2.2 Simplification and linearisation

A transfer function can simply model the dynamics of both diesel engines and electric propulsion systems in the s-domain in Hansen et al. (2001). For diesel engines, the input $Y(s)$ denotes the fuel pump command.

$$H(s) = \frac{M(s)}{Y(s)} = \frac{K}{Ts+1}e^{-\tau s} \tag{2}$$

The backstepping controller design could be applied for both fixed and controllable pitch propeller as long as the transition of pitch angle is smooth. In this paper, the variation of pitch angle is not simulated but will be further studied.

Assumption 1. The propeller pitch angle is regarded as a measurable parameter, that is $P = P_{des}$.

As we know, the propeller thrust and torque are nonlinearly dependent on the propeller rotational speed, pitch angle, propeller diameter, and propeller expanded blade ratio. From Wageningen B-Screw series, the thrust and torque coefficient K_T and K_Q are calculated as $K_T = f_T(n, \frac{P}{D}, J, \frac{A_E}{A_O}, R_n)$ and $K_Q = f_Q(n, \frac{P}{D}, J, \frac{A_E}{A_O}, R_n)$, where n is the propeller rotational speed $\frac{P}{D}$ is the pitch ratio, J is the advance number, $\frac{A_E}{A_O}$ is the expanded blade area ratio and R_n is the Reynolds number. These parameters are highly coupled. To enable design of backstepping control, simplification on the coefficients are discussed in Assumption 2.

Assumption 2. In the backstepping design, the propulsion coefficient K_T and K_Q are simplified as linearly dependent on the advance number J and the pitch angle in Fossen (2011). This gives K_T and K_Q the form of $K_T = (\alpha_1 - \alpha_2 J_a)p$ and $K_Q = (\beta_1 - \beta_2 J_a)p$. Thus, the propeller thrust and torque are $F_p = K_T \rho n_p^2 D^4$ and $M_P = K_Q \rho n_p^2 D^5$.

Assumption 3. In Figari and Altosole (2007), the ship resistance is simplified as a function of the ship speed v: $F_r = A_1 v + A_2 v^2 + A_3 v^3 + A_4 v^4 + A_5 v^5 + A_6 v^6$. Coefficients A_i $(i = 1, ..., 6)$ are to be determined for different ships and operating conditions.

Besides, the energy loss in the shaft transmission process is negligible. Thus, in the shaft and gearbox system, Assumption 4 is valid.

Assumption 4. The gear ratio for mechanical propulsion is defined as $r = \frac{n_e}{n_p}$ and the shaft torque from the engine side $rM_s = M_p$ based on the assumption of 100% efficiency of shaft and gearbox.

Assumption 5. The frictional torque tends to be proportional to the engine rotating speed with a static friction, that is $M_f = sign(n_e)M_{fs} + K_f n_e$, where $sign(.)$ is the sign function. Actually, the friction term is less significant on large thrusters used on surface vessels than on small thrusters typically used on underwater vehicles. In this paper, the static friction M_{fs} is neglected.

By following the linearisation and simplification of (1) in Assumption (1-4), the state-space equation representing the proposed ship speed tracking system is presented in (3).

$$\dot{x}_1 = -\sum_{i=1}^{6} a_i x_1^i - K^*_{\alpha_2} x_1 x_2 + K^*_{\alpha_1} x_2^2, \tag{3a}$$
$$\dot{x}_2 = K^*_{\beta_2} x_1 x_2 - K^*_{\beta_1} x_2^2 + x_3 + m_b - K^*_f x_2, \tag{3b}$$
$$\dot{x}_3 = -K_{e1} x_3 + u(t-\tau_d), \tag{3c}$$

where $[x_1, x_2, x_3]^T = [v, n_e, \frac{M_e}{2\pi I}]^T$ and $m_b = \frac{M_b}{2\pi I}$. The parameters are defined as $K^*_{\alpha_1} = \frac{\alpha_1 P \rho D^4}{Mr^2}$, $K^*_{\alpha_2} = \frac{\alpha_2 P \rho D^3 (1-w)}{Mr}$, $a_i = \frac{A_i}{M}$, $K^*_{\beta_1} = \frac{\beta_1 P \rho D^5}{2\pi I r^3}$, $K^*_{\beta_2} = \frac{\beta_2 P \rho D^4 (1-w)}{2\pi I r^2}$, $K^*_f = \frac{K_f}{2\pi I}$, $K_{e1} = \frac{1}{T}$.

The control objective is to track a desired ship speed $x_1 \to x_{1d}$ by controlling $u(t-\tau_d)$ and the electric torque M_b.

2.3 Electric power supply for high ship speed

In this paper, the torque from the electric motor is introduced into the hybrid propulsion system as auxiliary power supply for high speed navigation. We do not expect

the diesel engine to reach its maximal torque without any margin at any time. An equivalent model for the electric torque is expressed in (4), to avoid the saturation of engine torque.

$$M_b = K_p(M_e - \delta M_{emax}) + K_i \int_0^t (M_e - \delta M_{emax}) d\tau, \quad (4)$$

where M_{emax} is the maximal engine torque and $\delta = 0.95$ is the impact factor. In this paper, the hybrid power supply is only available for high ship speed $v > v_h$ and the engine torque reaches its upper bound $M_e > \delta M_{emax}$.

2.4 Problem Statement

The control strategy is designed based on the ship propulsion system with parameter decomposition in (3). The performance of the backstepping controller is tested in the nonlinear ship propulsion simulator where the parameters K_T and K_Q are derived from the Wageningen B-Screw series.

3. BACKSTEPPING CONTROLLER DESIGN AND STABILITY ANALYSIS

The controller will be developed using adaptive backstepping control law. To deal with input delay, we introduced Pade approximation in Lemma 6, and the radial basis function neural network (RBFNN) is used to handle pure-feedback problem in Lemma 7.

Lemma 6. The input delay models the delay of fuel injected to the diesel engine which is, in practice, short and can be estimated as $\tau_d \simeq \frac{2}{n_e}$. To deal with the short input delay, Pade approximation is introduced in the system, shown in (5).

$$\mathcal{L}\{u(t-\tau_d)\} = e^{-\tau_d s}\mathcal{L}\{u(t)\} \approx \frac{1-\tau_d s/2}{1+\tau_d s/2}\mathcal{L}\{u(t)\}. \quad (5)$$

For the system (3), if we introduce another variable x_4, the above Laplace transform is expressed as

$$\frac{1-\tau_d s/2}{1+\tau_d s/2}\mathcal{L}\{u(t)\} = \mathcal{L}\{x_4(t)\} - \mathcal{L}\{u(t)\}, \quad (6)$$

which gives

$$\begin{aligned} \dot{x}_4 &= -\gamma x_4 + 2\gamma u, \\ \gamma &= \frac{2}{\tau_d}. \end{aligned} \quad (7)$$

After the above transformation, the state x_4 is introduced in the state-space equations which becomes

$$\dot{x}_1 = f_1(\bar{x}_2) + x_2, \quad (8a)$$
$$\dot{x}_2 = f_2(\bar{x}_2) + x_3 + m_b, \quad (8b)$$
$$\dot{x}_3 = -\frac{1}{T}x_3 + x_4 - u, \quad (8c)$$
$$\dot{x}_4 = -\gamma x_4 + 2\gamma u. \quad (8d)$$

Before we starting the stability proof, the neural network approximation is introduced in the first state dynamics. Since the ship speed dynamics (x_1) is nonlinearly dependent on the shaft speed (x_2), we here use RBF-NN approximation to deal with such pure-feedback problem.

Lemma 7. The RBF network is used to approximate unknown smooth function $h(Z) : R^m \to R$. The approximation can be described as

$$h(Z) = W^\top \Phi(Z), \quad (9)$$

where $Z \in R^m$ is the neural network input vector, and $W = [w_1, w_2, ..., w_n]^\top \in R^n$ is the weight vector, and $\Phi(Z) \in R^n$ are radial basis functions which are chosen as

$$\phi_i(Z) = exp\left[-\frac{(Z-u_i)^\top (Z-u_i)}{\eta_i^2}\right], \quad (10)$$

where $u_i = [u_{i1}, u_{i2}, ..., u_{im}]^\top$ is the center vector and η_i is the width of Gaussian function. The Neural Network approximation in (9) can approximate any continuous function $h(Z)$ defined on the compact set Ω_Z with arbitrary precision ϵ in Gao et al. (2016).

$$h(Z) = {W^*}^\top \Phi(Z) + \epsilon, \qquad \forall Z \in \Omega_Z \subset R^m, \quad (11)$$

where W^* is the ideal weight vector and ϵ is the approximation error. The backstepping controller design is presented based on the coordinate transformations.

$$z_1 = x_1 - y_d, \quad (12a)$$
$$z_2 = x_2 - \alpha_1, \quad (12b)$$
$$z_3 = x_3 - \alpha_2 + \frac{1}{\gamma}x_4, \quad (12c)$$

where α_1 and α_2 are to be defined later.

Step 1: Substituting (8a) into z_1 yields

$$\begin{aligned} \dot{z_1} &= (\dot{x}_1 - \dot{y_d}) \\ &= f_1(\bar{x}_2) + x_2 - \dot{y_d} \\ &= f_1(\bar{x}_2) + z_2 + \alpha_1 - \dot{y_d}. \end{aligned} \quad (13)$$

In this step, the Lyapunov function candidate V_1 is defined as

$$V_1 = \frac{1}{2}z_1^2 + \frac{\tilde{\theta}_1^2}{2\beta_1}, \quad (14)$$

where $\tilde{\theta}_1 = \theta_1 - \hat{\theta}_1$, and $\dot{\tilde{\theta}}_1 = \dot{\hat{\theta}}_1$. The derivative of V_1 is

$$\dot{V}_1 = z_1\left[(f_1(\bar{x}_2) - \dot{y_d}) + z_2 + \alpha_1\right] - \frac{\tilde{\theta_1}\dot{\hat{\theta}}_1}{\beta_1}. \quad (15)$$

We use $H_1(Z_1) = {W_1}^\top \Phi_1(Z_1), \forall Z_1 \in \Omega_{Z_1}$, to approximate the smooth continuous function $f_1(\bar{x}_2) - \dot{y_d}$. By applying the Young's inequality, we have

$$\begin{aligned} z_1 H_1(Z_1) &= z_1({W_1^*}^\top \Phi_1 + \epsilon_1) \\ &= z_1 {W_1^*}^\top \Phi_1 + z_1\epsilon_1 \\ &\le \frac{z_1^2\|W_1\|^2\Phi_1^\top\Phi_1}{2a_1^2} + \frac{a_1^2}{2} + \frac{{z_1}^2}{2} + \frac{\epsilon_1^2}{2} \\ &\le \frac{z_1^2\theta_1\Phi_1^\top\Phi_1}{2a_1^2} + \frac{a_1^2}{2} + \frac{{z_1}^2}{2} + \frac{\epsilon_1^2}{2}, \end{aligned} \quad (16)$$

where $\theta_1 = ||W_1||^2$ and $Z_1 = [x_1, \hat{\theta}_1, y_d, \dot{y}_d]^\top$. The positive parameter a_1 comes from the Young's inequality, and can be chosen to adjust the control performance.

Then, substituting (16) into (15) yields

$$\begin{aligned} \dot{V}_1(x) \le\ & z_1\left(z_1\frac{\theta_1\Phi_1^\top\Phi_1}{2a_1^2} + \alpha_1 + z_2 \right. \\ & \left. + \frac{1}{2}z_1\right) - \frac{\tilde{\theta}_1\dot{\hat{\theta}}_1}{\beta_1} + \frac{a_1^2}{2} + \frac{\epsilon_1^2}{2}. \end{aligned} \quad (17)$$

$\hat{\theta}_1$ is the estimation of $||W_1||^2$. The first virtual control signal α_1 and adaptive law $\hat{\theta}_1$ are chosen as:

$$\alpha_1 = -(c_1 + \frac{1}{2})z_1 - \frac{z_1\hat{\theta}_1\Phi_1^\top\Phi_1}{2a_1^2}, \tag{18a}$$

$$\dot{\hat{\theta}}_1 = -m_1\beta_1\hat{\theta}_1 + \frac{\beta_1 {z_1}^2\Phi_1^\top\Phi_1}{2a_1^2}, \tag{18b}$$

where $c_1 > 0$ is the control gain. We can prove that $\hat{\theta}_1\tilde{\theta}_1 = \tilde{\theta}_1(\theta_1 - \tilde{\theta}_1) \leq -\frac{\tilde{\theta}_1^2}{2} + \frac{\theta_1^2}{2}$. Hence, the following inequality holds for step 1.

$$\dot{V}_1(x) \leq -c_1 {z_1}^2 - \frac{m_1\tilde{\theta}_1^2}{2} + z_1z_2 + \frac{a_1^2}{2} + \frac{\epsilon_1^2}{2} + \frac{m_1\theta_1^2}{2}. \tag{19}$$

Step 2: Substituting (8b) into z_2 yields

$$\begin{aligned}\dot{z_2} &= \dot{x}_2 - \dot{\alpha}_1 \\ &= f_2(\bar{x}_2) + m_b + x_3 - \dot{\alpha}_1 \\ &= f_2(\bar{x}_2) + m_b + z_3 + \alpha_2 - \frac{x_4}{\gamma} - \dot{\alpha}_1.\end{aligned} \tag{20}$$

The Lyapunov function $V_2(x)$ and its derivation of time are

$$V_2 = V_1 + \frac{1}{2}z_2^2, \tag{21a}$$

$$\dot{V}_2 = \dot{V}_1 + z_2\left(f_2(\bar{x}_2) + m_b + z_3 + \alpha_2 - \frac{x_4}{\gamma} - \dot{\alpha}_1\right) \tag{21b}$$

The virtual control signal α_2 is chosen as:

$$\alpha_2 = -c_2z_2 - f_2(\bar{x}_2) - m_b + \dot{\alpha}_1 - z_1 + \frac{x_4}{\gamma}, \tag{22}$$

where $c_2 > 0$ is the control gain. Then, the following inequality holds for step 2.

$$\begin{aligned}\dot{V}_2(x) \leq &-\sum_{k=1}^{2} c_k z_k^2 - \frac{m_1\tilde{\theta}_1^2}{2} + z_2z_3 + \frac{a_1^2}{2} + \frac{\epsilon_1^2}{2} \\ &+\frac{m_1\theta_1^2}{2}.\end{aligned} \tag{23}$$

Step 3: Different from formal steps, to handle input delays using pade approximation, substituting (8c) and (8d) into z_3 yields

$$z_3 = x_3 - \alpha_2 + \frac{1}{\gamma}x_4, \tag{24a}$$

$$\dot{z}_3 = \dot{x}_3 - \dot{\alpha}_2 + \frac{1}{\gamma}\dot{x}_4 = -\frac{1}{T}x_3 + u - \dot{\alpha}_2. \tag{24b}$$

The Lyapunov function $V_3(x)$ and its derivation of time are

$$V_3 = V_2 + \frac{1}{2}z_3^2, \tag{25a}$$

$$\dot{V}_3 = \dot{V}_2 + z_3\left(-\frac{1}{T}x_3 - \dot{\alpha}_2 + u\right). \tag{25b}$$

The final control signal u is chosen as:

$$u = -c_3z_3 + \frac{1}{T}x_3 + \dot{\alpha}_2 - z_2. \tag{26}$$

Hence, the following inequality holds for the whole system.

$$\dot{V}_3(x) \leq -\sum_{k=1}^{3} c_k z_k^2 - \frac{m_1\tilde{\theta}_1^2}{2} + \frac{a_1^2 + \epsilon_1^2}{2} + \frac{m_1\theta_1^2}{2}, \tag{27}$$

where θ_1, a_1 and ϵ_1 are assumed to be bounded. Considering the analysis results in (27) of the Lyapunov function, the stability of the closed-loop system can be establised if Theorem 8 satisfies.

Theorem 8. If there exist a positive R, and a bounded and positive δ such that $\dot{V} \leq -RV + \delta$, the proposed control scheme with adaptive backstepping control law ensures that all signals in the close-loop system are uniformly ultimately bounded.

Proof.

Define

$$\begin{aligned}R &= min(2c_1, 2c_2, 2c_3, m_1\beta_1), \\ \delta &= \frac{a_1^2}{2} + \frac{\epsilon_1^2}{2} + \frac{m_1\theta_1^2}{2},\end{aligned} \tag{28}$$

where $R > 0$ and $\delta > 0$. Thus, from (27), we obtain

$$\dot{V} \leq -RV + \delta. \tag{29}$$

Then, by direct integration of the differential inequality (29), we have

$$\begin{aligned}V &\leq V(0)e^{-Rt} + \frac{\delta}{R}(1 - e^{-Rt}) \\ &\leq (V(0) - \frac{\delta}{R})e^{-Rt} + \frac{\delta}{R},\end{aligned} \tag{30}$$

which shows that V is uniformly bounded, and thus the tracking error z_1 is also bounded. □

Therefore, from following the Theorem 8, it can be concluded that the closed-loop system is uniformly ultimately bounded and the tracking error $x_1 - y_d$ is bounded, which could be reduced to a small neighborhood of the origin via tunning the controller gain, parameters of RBF-NN approximation and updating law.

Remark 9. In theory, the tracking error could becomes very small by tuning parameters a_1 and m_1. This is restricted by the performance of RBF-NN approximation: For too small parameters, it cannot estimate the goal function properly.

4. SIMULATION: SHIP SPEED TRACKING AND PROPULSION SYSTEM

4.1 Backstepping controller design

The control parameters are listed in Table B.1. The parameters c_i are the control gains: The tracking error decreases by increasing control gains. To address the unknown nonlinear function $f_1(\bar{x}_2)$ in (8a), the RBF neural network function are used in the form of (10). The initial parameters in (10) used are $\eta = [3\,6\,2\,3\,2\,4\,3]$ ($\eta_i = \eta(i)$), and the matrix u, where $u_i = u(:, i)$.

$$u = \begin{bmatrix} 1 & 0 & 1 & 1 & 0 & 0 & 0 \\ 0.1 & 0.2 & 0.5 & 1 & 1 & 0 & 0 \\ 0 & 0 & 1 & 0 & 0 & 0 & 1 \\ 0.2 & 0.1 & 0.1 & 0.2 & 0.5 & 0.01 & 0.01 \end{bmatrix}. \tag{31}$$

The vector u_i is initialized close to the initial value of input vector Z, such that the Gaussian function can be effectively mapped from the starting time. The parameters η and u are updated using the gradient descent method in each sampling time.

4.2 Nonlinear simulator settings

As stated in Assumption 2, the open water coefficient K_T and K_Q are linearised and used to construct the backstepping controller. In this paper, the nonlinear K_T derived from a Wagningen B4-55 propeller and its linearisation

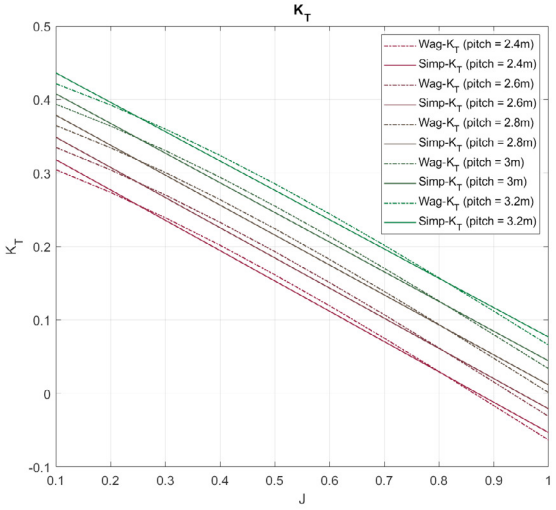

Fig. 1. Plot of open-water coefficient K_T and its linearization

are illustrated in Fig.1. Similar linearisation for the torque coefficient K_Q are carried out as well.

The characteristics of the ship is listed in Table A.1. Together with the total resistance coefficients derived from the calm water tests, the resistance curve for the ship is estimated and used in the simulation after curve fitting based on Assumption 3.

4.3 Simulation results

The tracking performance of the backstepping controller is displayed in Fig. (2-8). It is shown in Fig. 3 that the tracking error oscillates between $e = -0.035[m/s]$ which is satisfactory for actual implementation. The tracking error mainly comes from the application of RBF-NN in the adaptive backstepping control, where the ship speed (x_1) is proven to be in the small neighborhood of the desired speed (y_d). However, since the RBF Neural Network can never approximate the goal function without any deviation, it is inevitable to see zero tracking error. Another reason of the non-zero tracking error is the difference between the controller design for linearised ship propulsion model an the simulation on nonlinear ship dynamics.

From Fig. 4, we can see that when the engine torque exceeds its maximal value, the PI control of battery torque is activated until the required torque is less than the maximal engine torque. The PI controller gain is presented in Table. B.2. The control input from the backstepping algorithm is shown in Fig. 5. Fig. 6 shows the actual and RBF-approximated values of $(f_1(\bar{x}_2) - \dot{y}_d)$. Fig. 7 presents the relative error of RBF approximation. In Fig. 6 and Fig. 7, the RBF approximates the target function with very small deviation and presents satisfactory results. Fig. 8 presents the variance of advance number J during simulation. As stated before, the advance number mainly fluctuates between [0.6, 0.8] in the presented simulation, where the linearisation of thrust and torque coefficients is valid.

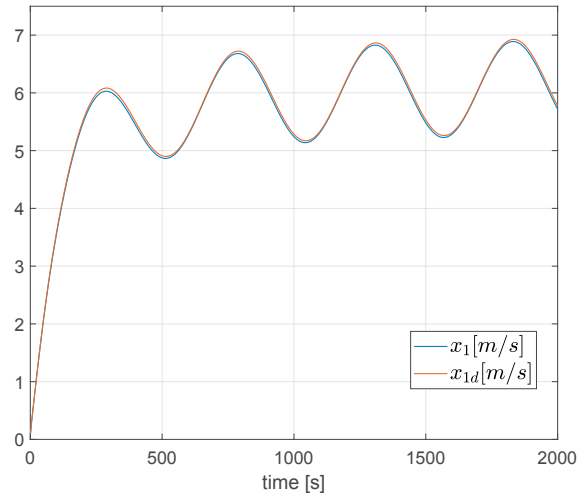

Fig. 2. Plot of speed tracking x_1 and y_d

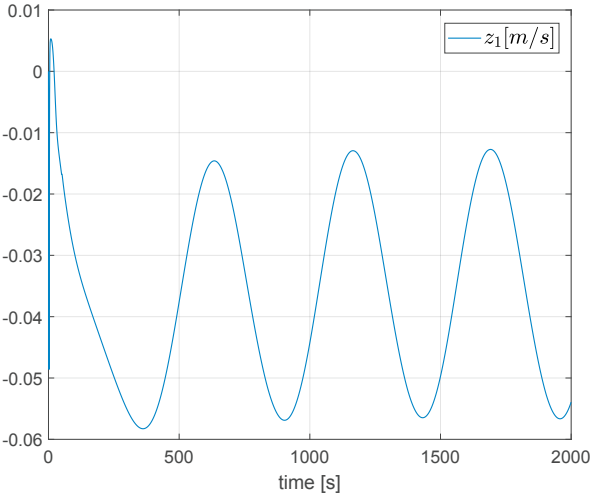

Fig. 3. Plot of speed tracking error e_1

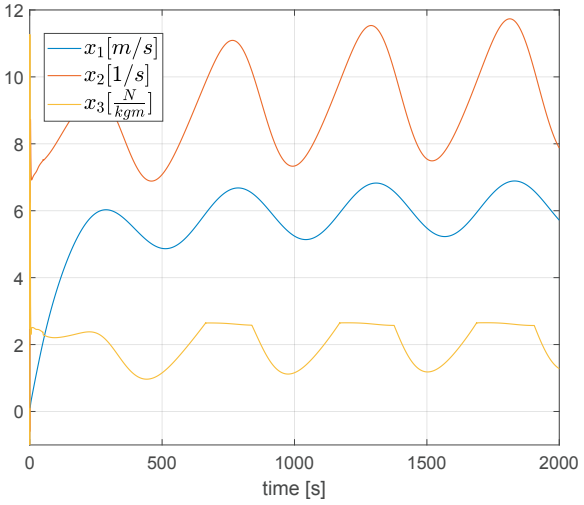

Fig. 4. Plot of all states x

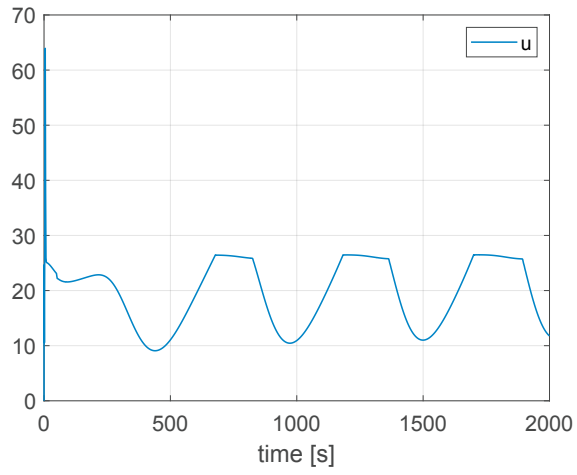

Fig. 5. Plot of control input u

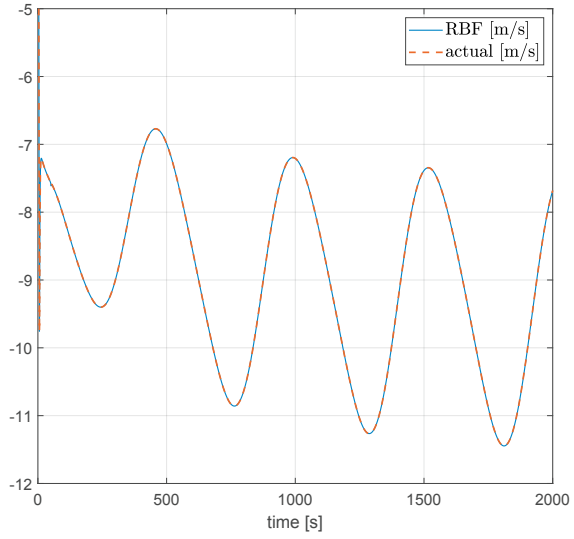

Fig. 6. Plot of neural network approximation

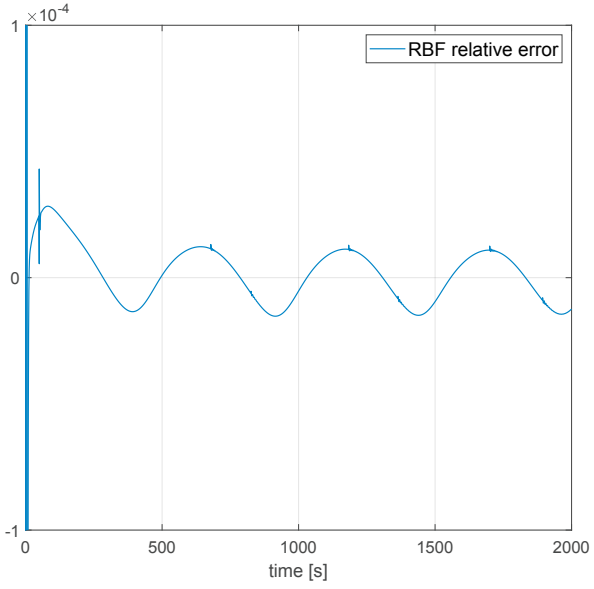

Fig. 7. Plot of neural network relative approximation error

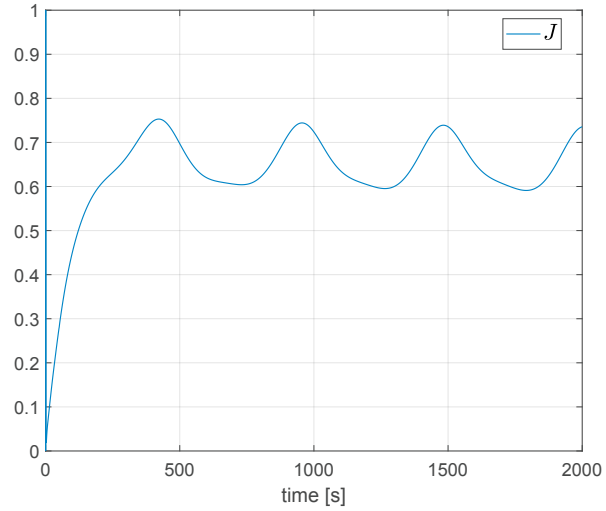

Fig. 8. Plot of advance coefficient J

5. CONCLUSION

In this paper, an adaptive backstepping tracking control for the ship propulsion system was proposed. Using RBF-NN neural network, the nonlinear ship speed tracking dynamics was well-approximated. The Pade approximation estimated the fuel injection delay with negligible deviation. It was proven that all states of the proposed system are uniformly ultimately bounded, and the tracking error ultimately converged to a small neighborhood of the origin. In future works, the accurate dynamics of battery and electric motor will be considered.

ACKNOWLEDGEMENTS

This work was supported by the Research Council of Norway through the SEAOPS project of Brunvoll AS, project number 309660, and through the Centre of Excellence funding scheme, project number 223254, AMOS. Optimal combinator curve data and calm water test support from Sintef Oceans is gratefully acknowledged.

REFERENCES

Figari, M. and Altosole, M. (2007). Dynamic behaviour and stability of marine propulsion systems. *Proceedings of the Institution of Mechanical Engineers, Part M: Journal of Engineering for the Maritime Environment*, 221(4), 187–205.

Fossen, T.I. (2011). *Handbook of marine craft hydrodynamics and motion control*. John Wiley & Sons.

Gao, Y.F., Sun, X.M., Wen, C., and Wang, W. (2016). Observer-based adaptive nn control for a class of uncertain nonlinear systems with nonsymmetric input saturation. *IEEE transactions on neural networks and learning systems*, 28(7), 1520–1530.

Ge, S.S. and Wang, C. (2002). Adaptive nn control of uncertain nonlinear pure-feedback systems. *Automatica*, 38(4), 671–682.

Geertsma, R., Negenborn, R., Visser, K., and Hopman, J. (2017). Design and control of hybrid power and propulsion systems for smart ships: A review of developments. *Applied Energy*, 194, 30–54.

Hansen, J.F., Ådnanes, A.K., and Fossen, T.I. (2001). Mathematical modelling of diesel-electric propulsion systems for marine vessels. *Mathematical and Computer Modelling of Dynamical Systems*, 7(3), 323–355.

Li, H., Wang, L., Du, H., and Boulkroune, A. (2016). Adaptive fuzzy backstepping tracking control for strict-feedback systems with input delay. *IEEE Transactions on Fuzzy Systems*, 25(3), 642–652.

Liu, Y.J. and Tong, S. (2016). Barrier lyapunov functions-based adaptive control for a class of nonlinear pure-feedback systems with full state constraints. *Automatica*, 64, 70–75.

Ma, J., Xu, S., Li, Y., Chu, Y., and Zhang, Z. (2018). Neural networks-based adaptive output feedback control for a class of uncertain nonlinear systems with input delay and disturbances. *Journal of the Franklin Institute*, 355(13), 5503–5519.

Mestemaker, B., Castro, M.G., van den Heuvel, H., and Visser, K. (2020). Dynamic simulation of a vessel drive system with dual fuel engines and energy storage. *Energy*, 194, 116792.

Miyazaki, M.R., Sørensen, A.J., and Vartdal, B.J. (2016). Reduction of fuel consumption on hybrid marine power plants by strategic loading with energy storage devices. *IEEE Power and Energy Technology Systems Journal*, 3(4), 207–217. doi:10.1109/JPETS.2016.2621117.

Vrijdag, A. and Stapersma, D. (2017). Extension and application of a linearised ship propulsion system model. *Ocean Engineering*, 143, 50–65.

Xiros, N. (2012). *Robust control of diesel ship propulsion*. Springer Science & Business Media.

Yu, H., Xie, T., Paszczynski, S., and Wilamowski, B.M. (2011). Advantages of radial basis function networks for dynamic system design. *IEEE Transactions on Industrial Electronics*, 58(12), 5438–5450.

Zhao, Z., Yang, Y., Zhou, J., Li, L., and Yang, Q. (2018). Adaptive fault-tolerant pi tracking control for ship propulsion system. *ISA transactions*, 80, 279–285.

Appendix A. MAIN CHARACTERISTICS OF THE SHIP

Table A.1. Parameters of the ship

Parameters	Symbol	Value
Length betw. perp.	L_{PP} [m]	55.8
Volume displacement	$\bigtriangledown$ [m^3]	ca. 2600
Wetted surface	S [m^2]	ca. 1200

Appendix B. PARAMETERS USED IN SIMULATION

Table B.1. parameters of backstepping controller

Parameters	Value	Parameters	Value
c_1	30.0	a_1	0.1
c_2	15.0	m_1	0.01
c_3	2.0	β_1	0.1

Table B.2. parameters of PI controller

Parameters	Value
K_p	0.1
K_i	0.2